COLLOIDAL QUANTUM DOT BASED LIGHT EMITTING DEVICES ON SILICON SUBSTRATE

BY

SHIUL KHADKA

THESIS

Submitted in partial fulfillment of the requirements
for the degree of Master of Science in Electrical and Computer Engineering
in the Graduate College of the
University of Illinois at Urbana-Champaign, 2013

Urbana, Illinois

Adviser:

Professor Ann Catrina Coleman

Abstract

Light sources based on silicon have been the subject of interest for many years. Silicon would not only provide high volume manufacturing for commercialization but also allow complementary metal–oxide–semiconductor (CMOS) compatibility enabling integration of light sources within CMOS circuitry. Colloidal semiconductor nanocrystals have narrow emission spectra which makes them an excellent choice for active media in optoelectronic applications. Moreover, solution processability of colloidal quantum dots makes processing and integration on the silicon platform easier. This thesis discusses the design and fabrication of colloidal quantum dot based light-emitting devices using inorganic materials on a silicon platform for visible wavelengths. The results demonstrate the ability to integrate colloidal quantum dots on silicon which would allow the development of compact light sources for optical communication.

Acknowledgment

I would like to express my sincere gratitude to Prof. Ann Catrina Coleman for giving me this opportunity to be a part of her research group at the University of Illinois. I am grateful to her for giving me the freedom to think independently and try out different ideas and for helping me to become a better researcher. Without her support and guidance, this thesis would not have been possible. Meetings with Prof. James Coleman was a great privilege and his passion for science always motivated me to work harder. I am very thankful for the training and support provided by MNTL superusers: Dr. Edmond Chow, Yaguang Lian, Hal Romans and Mike Hansen.

Many thanks to all the members of the Semicondutor Laser group: Runyu Liu, JD Kim, Yun Lu, Pavel Liudvih and Nick Choi. Working in the lab would not have been fun, easier and productive without you guys and I really appreciate all the help and encouragement that I received during my time in the lab. I would also like to thank Dr. Sun Jun Lim for his freindship, valuable advise and constant encouragement.

Finally, I would like to extend my gratitude and love to my family for always being there as a major source of inspiration and for their unconditional support.

Contents

Chapter 1

Introduction

1.1 Silicon Photonics

Silicon photonics is a new approach to using light to transmit data instead of electrical signals. The ever-increasing demand for greater bandwidth, extraordinary scalability of optical fiber, failure of copper to scale higher speeds, and the ability to transmit energy more efficiently using light rather than electricity is the driving force behind silicon photonics. Moreover, due to its compatibility with the mature integrated circuit (IC) manufacturing industry, silicon photonics offers the potential of creating low-cost photonics for mass market applications [1]. The development of CMOS-integrated optical devices such as wavelength division multiplexers, electro-optical modulators, photodetectors and fiber edge couplers has allowed monolithic integration of deeply scaled optical circuits [2].

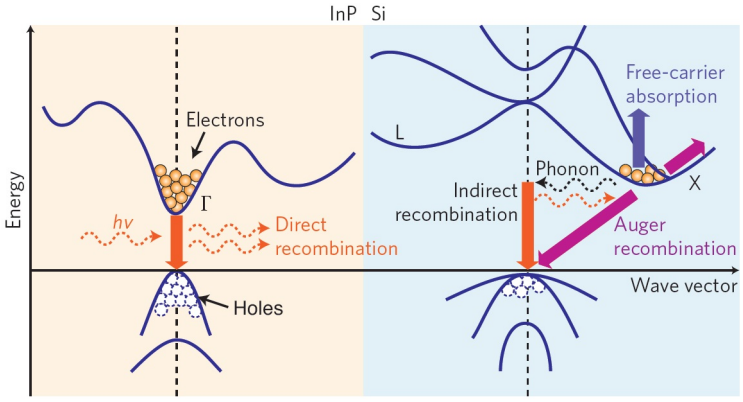

Figure 1.1: Energy band diagrams and carrier transition processes in indium phosphide (InP) (left) and silicon (right) [3].

Light sources such as LEDs (light-emitting devices) and lasers form an integral part of optical transceivers [2] but silicon-based light sources have remained one of the main challenges for silicon photonics as silicon is a poor light emitter. Silicon has an indirect bandgap (Figure 1.1, right) where the bottom of the conduction band is not aligned with the top of valence band along the wave vector because they have different momenta. A photon with energy near the semiconductor bandgap is massless which means it has almost zero momentum. Since these photons cannot carry crystal momentum, it requires a third particle to satisfy the conservation of crystal momentum. Therefore, the electrons need to wait for the absorption or emission of a phonon with extra momentum in order to recombine with a hole. This process reduces the probability of radiative recombination and increases the probability of non-radiative recombination where excess energy is released as a phonon to the semiconductor crystal lattice rather than a photon. The two main non-radiative recombination processes in direct semiconductors are Auger recombination and defect generated non-radiative recombination. Auger recombination occurs when an electron or hole is excited to a higher energy level by absorbing the released energy from an electron-hole recombination [3]. Despite this, silicon-based light-emitting devices have been demonstrated using high-quality bulk silicon inserted in a forward biased solar cell [4], stimulated Raman scattering in silicon waveguides [5], ion implantation in a silicon p-n junction [6], silicon nanocrystals in a dielectric matrix [7], and Er (Erbium) coupled to silicon nanocrystals in a dielectric [8]. However, these methods have their disadvantages such as low gain, unsuitable wavelength region for optical communication, and room temperature operation issues.

Unlike silicon, compound semiconductors such as InP have a direct bandgap i.e. the bottom of the conduction band is aligned with the top of the valence band. This increases the probability of radiative recombination which means that an electron-hole recombination almost always results in photon emission. A number of techniques based on compound semiconductor with a silicon platform have been proposed to address the light source issue. A hybrid silicon laser is one example where a III-V material is transferred to the silicon

wafer through bonding [9] or epitaxial growth [3]. However, this technique is hindered by the incompatibility of III-V material with the CMOS process, low yield due to bonding issues [10] and additionally, alignment of III-V lasers on silicon is time consuming and costly. Therefore, in this thesis, light sources based on the colloidal quantum dot with an integrated silicon platform is presented.

1.2 Semiconductor Nanocrystals for Photonic Applications

Semiconductor nanocrystals, also known as colloidal quantum dots (QDs), are solution-processed semiconductors which exhibit unique optical properties due to the quantum confinement effect. Colloidal QDs are chemically synthesized and have dimensions in the order of 1-10 nm. Colloidal QDs share similar physics principles compared to epitaxially grown QDs, except that they exhibit some distinct advantages such as stronger carrier confinement, larger excitonic interaction between the electrons and holes, and slower radiative times all owing to their smaller size [11]. They also have high monodispersivity and allow great control over shape and composition compared to the epitaxially grown QDs [11]. In addition, they exhibit a high quantum yield, narrow emission spectrum, and strong optical absorption which has made them useful in a wide range of applications such as fluorescent labeling, LEDs, and solar cells [11, 12, 13].

The narrow tunable emission spectra [13], and high photo-luminescence efficiency [14] make colloidal QDs potentially the most practical candidates for making quantum-dot light-emitting devices (QD-LEDs) [15]. In the last decade or more, a considerable amount of research has been focused on developing highly efficient QD-LEDs. Since the first demonstration in 1994, the efficiency of QD-LEDs has increased from 0.01% to a recent report of 18% [15]. QD-LEDs have great potential for being used for energy-efficient high color quality thin-film display and solid-state lighting [16]. The wide absorption spectrum, bandgap tun-

ability and cheap solution processibility make colloidal quantum-dot a promising candidate for solar cells as well. Additionally, solution-processed quantum dot allows processing onto light-weight flexible substrates through spin coating, spray-coating, reel-to-reel printing and inkjet printing which can potentially reduce the fabrication and packaging cost [16].

Along with applications for LEDs and solar cells, a significant amount of work has been conducted in using colloidal QDs for making lasers and photodetectors. Lasing from colloidal QDs is extremely difficult due to the requirement of high packing density and losses due to non-radiative recombination [16]. The key principle in the operation of a laser is stimulated emission. Materials capable of lasing have high energy states that are "metastable" and can hold their higher energy state for a longer time before decaying spontaneously. For stimulated emission, a condition of population inversion needs to be satisfied. Population inversion occurs when there are more electrons in the higher energy state than there are in the lower energy state. The population inversion condition leads to optical gain which occurs when stimulated emission overcomes absorption and losses. Recently, optical gain from colloidal QD was reported using densely packed films of CdSe QDs but the non-radiative process such as Auger recombination and short relaxation rate in such films reduces the lifetime of population inversion and makes lasing from nanocrystals extremely difficult [17]. Besides laser, much progress has also been done in using colloidal QDs for photodetector and infrared imaging applications. Various photodetector structures have been reported using the tunable property of the colloidal QD. Few such examples are detectors integrated with silicon backplanes with an operating wavelength of 1310 nm [18], colloidal HgTe quantum dot photodetectors with a room-temperature photoresponse beyond 5 µm [19], and there have been reports of photodetectors that use multi-exciton generation for high efficiency [20].

In summary, the potential of colloidal QDs for application in full-color video, solid-state lighting, next-generation solar cells, detector arrays, and lasers make them one of the most attractive candidates for photonic applications.

1.3 Aim of the Work

The goal of this work is to investigate compact light sources with an ability to integrate with silicon, which is compatible with CMOS technology. As mentioned earlier, silicon with an indirect bandgap is a poor light emitter but it is still the most widely used material in the semiconductor industry. Development of light sources based on silicon would allow the use of established advanced CMOS technology which would not only facilitate high volume production but also reduce cost significantly. Semiconductor nanocrystals with their wide tunability, high photo-luminescence (PL) efficiency and solution processibility, are a very attractive candidate for integration with silicon for the development of a compact low-cost light source. The small size and the ease of integration would allow monolithic integration of the light source for interchip communication. The ability to integrate compact light sources based on colloidal QDs to a CMOS circuit will not compromise the performance of the electronics because it does not require special fabrication steps. The fabrication of the light source itself might not be a current CMOS process but it would not require processing that would introduce steps which would affect the CMOS chip.

This thesis describes the work carried out toward the goal of integrating colloidal QDs with silicon. In this thesis, various patterning methods, design, fabrication and electroluminescence (EL) tests of basic colloidal QD LEDs have been reported.

1.4 Thesis Outline

Chapter 1 of this thesis provides an introduction and explains the motivations behind using colloidal QDs as an active material for fabrication of LEDs. Chapter 2 provides background theory with an explanation of unique optical and electrical properties of quantum dots. Here, the basic physics of LED devices along with the choice of material for designing efficient colloidal QD-LEDs is also described. Chapter 3 provides an overview of the fabrication of the

device starting from the synthesis of colloidal QDs. This chapter describes various deposition techniques of colloidal QDs, patterning of colloidal QDs and fabrication of LEDs with colloidal QD as an active emitter on a silicon backplane. Chapter 3 also includes characterizations of colloidal QDs used for fabricating LEDs along with some device characterization. Finally, Chapter 4 summarizes the thesis with some suggestions for future work.

Chapter 2

Background Theory and Device Design

2.1 Quantum Confinement in Quantum Dots

Quantum dots have a radius smaller than the characteristic Bohr exciton radius which gives rise to quantum confinement effects. This results in confinement of the carriers in all three directions and changes the density of states. Unlike bulk semiconductors, which have a continuous density of states, the three-dimensional (3D) quantization in a quantum dot gives rise to a delta-shaped density of states with no states in between the delta peaks. Therefore, these quantum dots which are small enough bits of semiconductor use physical confinement to approach atom-like behavior [21]. This is similar to the elementary problem of "the particle in the box" in quantum mechanics.

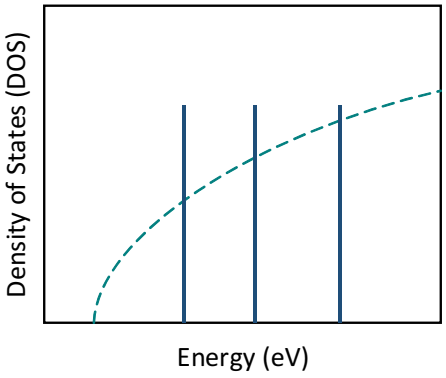

Figure 2.1: Schematic diagram illustrating the representation of the electronic density of states (DOS) of quantum dots (delta-like peaks) and bulk semiconductors (dashed).

For a quantum dot, an electron confined in all directions has no free motion which results in no k-space being available for free electrons to occupy. Therefore, each quantum state of a zero-dimensional (0D) system such as this can be occupied by only two electrons. The density of states is thus described by the delta function as follows:

$$D^{(0)}(E) = 2\delta(E - E_c) \tag{2.1}$$

For more than one quantum state, the density of states is given by

$$D^{(0)}(E) = \sum_n 2\delta(E - E_c) \tag{2.2}$$

The density of states for the quantized 0D electron system was shown in Figure 2.1. The density of states is further applied to both the valence band and conduction band of a material to obtain the joint density of states (JDOS). The JDOS determines the optical and electronic properties of the material.

2.2 Optical Properties of Colloidal Quantum Dots

The optical properties, such as absorption and emission, of the colloidal QDs are governed by the quantum confinement effect as described in section 2.1. The optical properties of colloidal QDs change with size. This basic phenomenon can be understood by considering the uncertainty relation between position and momentum for free and confined particles. For a free particle, momentum can be precisely defined whereas the uncertainty in position increases. For a confined particle, the uncertainty in position decreases while momentum uncertainty increases. This allows us to view discrete energies of a particle as a superposition of bulk momentum states which results in compression of nearby transitions allowing single intense transition in the particle [22].

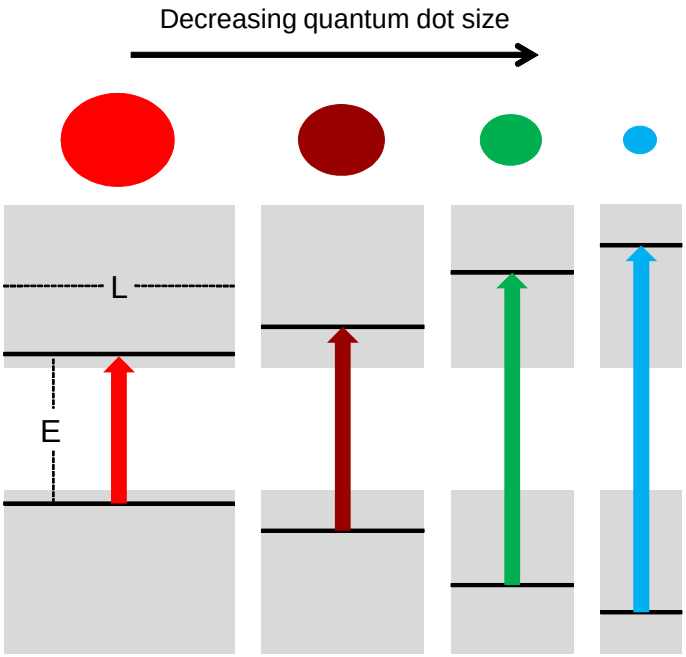

Figure 2.2: Schematic of the effect of the decreased size of the box or the dot on the increased energy gap of a semiconductor quantum dot. Decrease in size (from left to right) shows increase in bandgap and decrease in wavelength of light emitted.

The effect on optical properties due to the change in bandgap energy with change in size can be further understood by modeling the quantum dot using "particle in the spherical well" where the potential inside the well is zero. Brus developed the approximate relationship between the energy bandgap and particle size [23] and the relationship for the lowest excited state energy is given by:

$$E = E_{bulk} + \frac{\hbar^2 \pi^2}{2a^2}\left(\frac{1}{m_e^*} + \frac{1}{m_h^*}\right) - \frac{1.8e^2}{4\pi\epsilon\epsilon_0 a} + polarization\, terms \tag{2.3}$$

where E is the energy of the first excited electronic state, E_{bulk} is the bandgap of the bulk material, $\hbar$ is Planck's constant, a is the radius of the quantum dot, m_e^* is the effective mass of the electron for the material, m_h^* is the effective mass of the hole for the material, e is the charge of the electron, ϵ_0 is the permittivity of free space, and ϵ is the relative permittivity of the material. In eq. (2.3), the first term defines the bandgap of the bulk

material, the second term is quantum energy due to localization, and the third term is the Coulomb attraction between the electron and the hole with polarization terms. Equation (2.3) clearly shows the dependence of the bandgap on the inverse square of the radius of the quantum dot. Therefore, with the decrease in the size of the quantum dot, the energy of the particle increases, causing it to absorb light at shorter wavelengths as shown in Figure 2.2.

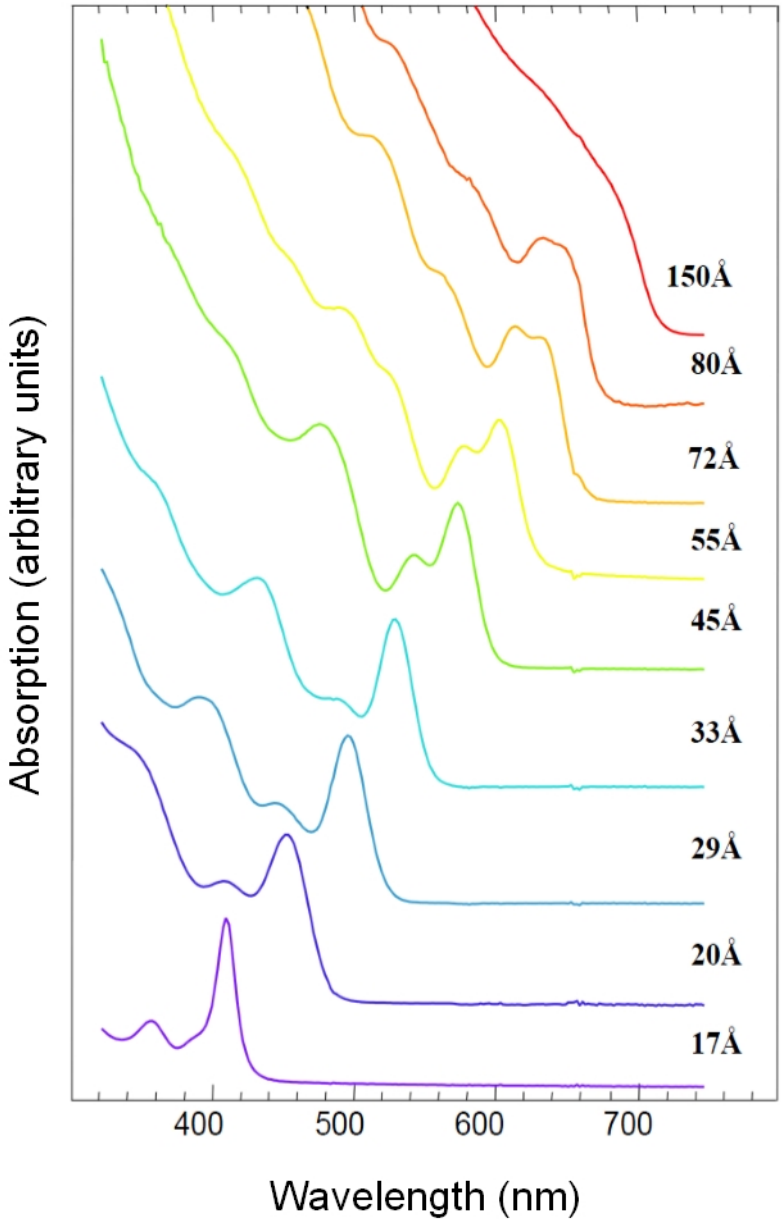

Figure 2.3: Absorption spectra of CdSe quantum dots with diameter varying from 17 A° to 150 A° [24].

As an example, absorption spectra of CdSe ranging from size 1.7 nm to 15 nm along with sharp interband transitions are shown in Figure 2.3. It can be clearly seen in the graph that with the decrease in size of quantum dots, the bandgap increases as represented by the blue shift of the absorption curve. The variation in the size of CdSe quantum dots can result in a tunabilility of the bandgap from 3.1 eV to 1.8 eV which corresponds to a shift in wavelength from 400 nm to 700 nm. This change in bandgap is significant compared to the bandgap of bulk CdSe (1.73 eV).

Therefore, size-dependent bandgap tunability of QDs allows tuning of fluorescence emission across a broad wavelength range of 400–2000 nm, spanning from the near ultraviolet into the near-infrared. This optical property of colloidal QDs makes them very attractive for a variety of photonic applications.

2.3 Electrical Properties of Colloidal Quantum Dots

This section describes the electrical transport and transfer of charges in colloidal QD films. Due to strong confinement in nanocrystals, electron transport is limited to interparticle transfer rather than transport within a single particle [25]. This mechanism of charge transport is different than traditional semiconductor transport. This transport can be modeled as the charge transport in molecular systems where transport between nanocrystals is a result of hopping between localized states. In this section, Marcus theory [26] of electron transfer between localized states is explained and used for understanding the charge transfer between two nanocrystals. In Figure 2.4, the two parabolas represent the initial and the final states as a function of nuclear coordinates. The initial and the final states have different nuclear coordinates because there is a change in the charge of the atoms or molecules involved during an electron transfer. The electron transfer occurs at the intersection of the parabolas since the nuclear coordinates cannot change during the electron transfer process from initial to final state [25].

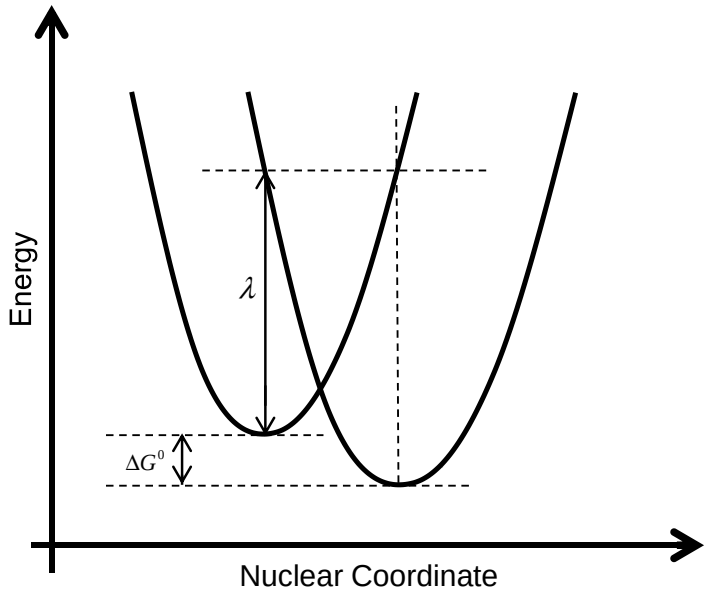

Figure 2.4: Energy as a function of nuclear coordinate for the initial and final states.

ΔG^0 is the free energy change between the initial and the final state and λ is the reorganization energy. The reorganization energy is the amount of energy required to force the final state to have the same nuclear configuration as the initial state without letting the electron transfer. The electron transfer rate constant as derived by Marcus et al. [27] is given by

$$k = \left(\frac{2\pi}{\hbar}\right) |V_{12}|^2 \left(4\pi^2 \lambda k T\right)^{-\frac{1}{2}} e^{-\frac{\Delta E}{kT}} \tag{2.4}$$

where

$$\Delta E = \frac{\left(\Delta G^0 - \lambda\right)^2}{4\lambda} \tag{2.5}$$

In eqs. (2.4) and (2.5), V_{12} is the electronic coupling matrix element between initial and final states on resonance and ΔE is the energy of the electron transfer. The total reorganization energy λ is the sum of λ_i and λ_0 which are the energies due to internal vibrations and changes in the configuration of the dielectric matrix surrounding the nanocrystals. Therefore,

$$\lambda = \lambda_i + \lambda_0 \tag{2.6}$$

The dielectric contribution is estimated using a dielectric continuum model whereas the transfer between two nanocrystal spheres is given by

$$\lambda_0 = \frac{e^2}{4\pi\epsilon_0}\left(\frac{1}{2r_1}+\frac{1}{2r_2}-\frac{1}{d}\right)\left(\frac{1}{\epsilon_{op}}-\frac{1}{\epsilon_s}\right) \tag{2.7}$$

where r_1 and r_2 are the radii of the two nanocrystal spheres, d is the distance of separation between two spheres measured from the center, and ϵ_{op} and ϵ_s are the optical and static dielectric constants of the surrounding insulating matrix respectively. Klimov estimated the value of λ_0 to be 100 meV for 2 mm CdSe nanocrystals with $d = 3.3$ mm which is the distance of separation for nanoparticles coated with tri-n-octylphosphine oxide (TOPO) using eq. (2.6) [25]. In this calculation, the values of static dielectric constant $\epsilon_s = 2.61$ and optical dielectric constant $\epsilon_{opt} = 2.07$ were used.

This analysis ignores the effect of disorder and trap states. But, it is important to note that nanocrystalline films are highly sensitive to disorder in energy levels which arise due to the distribution in particle sizes, distribution in the separation of nanocrystal spheres and the surrounding dielectric matrix [25]. Here, the electron tunneling process along with the role of internal dielectric relaxation in electron transfer dynamics were demonstrated. Besides the theoretical analysis of electron transfer dynamics, various experimental techniques such as measurement of the luminescence spectrum, transient absorption methods exist to characterize electron transport and transfer in nanocrystalline films. A theoretical understanding of electron transport and transfer dynamics is fundamentally essential for the design of practical nanocrystal-based optoelectronic devices such as LEDs.

2.4 Physics of LEDs

LEDs or light-emitting diodes are semiconductor light sources used for a wide range of photonic applications such as displays, lighting, communication etc. Traditionally, LEDs are

pn junction diodes made from direct band semiconductors, typically from III-V materials such as GaAs. With the application of a forward bias across the pn junction, electrons and holes are pushed toward the junction. This results in the formation of electron-hole pairs which eventually recombine producing light. The wavelength of light emission depends on the bandgap of the material. Furthermore, double heterostructure devices are used to improve the efficiency. A double heterostructure consists of a junction between materials of different bandgaps which creates localized jumps in the energy band diagram. This potential energy discontinuity provides a barrier and allows confinement of charge carriers in the lower bandgap material. This significantly increases current injection efficiency and lowers the threshold current of LEDs, lasers etc. Other various LED structures with semiconductor organic material and colloidal QDs as active material have emerged. The focus of this thesis is colloidal QDs, therefore, the major focus here will be on LEDs based on colloidal QDs.

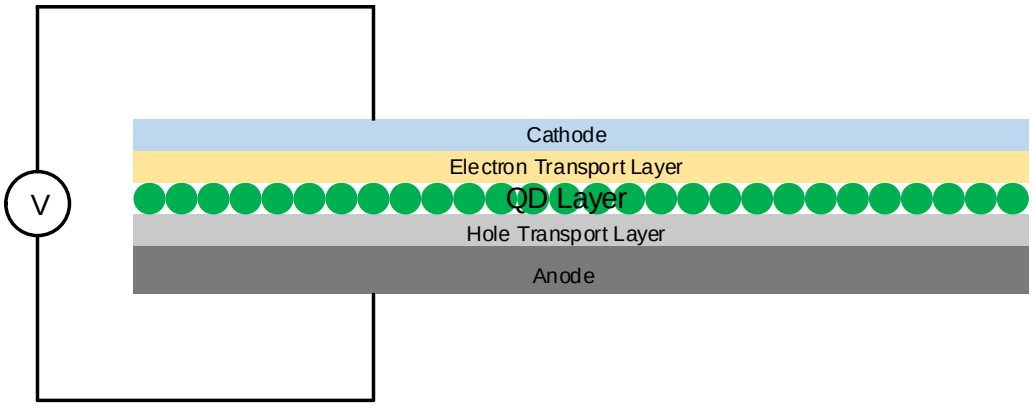

Figure 2.5: Typical QD-LED structure.

This thesis describes the basic structure and operation of a colloidal QD-LED. A generalized colloidal QD-LED device structure as shown in Figure 2.5, consists of an active emitting layer of colloidal QDs sandwiched between a electron transport layer (ETL) and a hole transport layer (HTL) with a metallic cathode and semitransparent anode through which light is emitted. Various structures are possible based on the selection of ETL and HTL that sandwich the QD layer. A few examples are organic-organic, inorganic-organic, and inorganic-inorganic layers of ETL-HTL respectively. The highest efficiency has been

obtained from a hybrid organic-inorganic charge transport layer structure. In such a structure the inorganic charge transport layer is usually a metal oxide whereas an organic charge transport layer is an organic semiconductor. Charges are injected into the active layer of colloidal QDs by applying an electric field between the two metallic electrodes whose work functions are chosen to facilitate injection. The holes are injected from the HTL whereas electrons from the ETL as shown in Figure 2.5. Both HTL and ETL are chosen to improve the efficiency of hole and electron injection respectively which in turn increases the probability of radiative recombination in the active layer. In addition, there have been reports on cross-linking the colloidal QD layer which significantly reduces the charge injection barriers and thus, increases the performance of colloidal QD-LEDs.

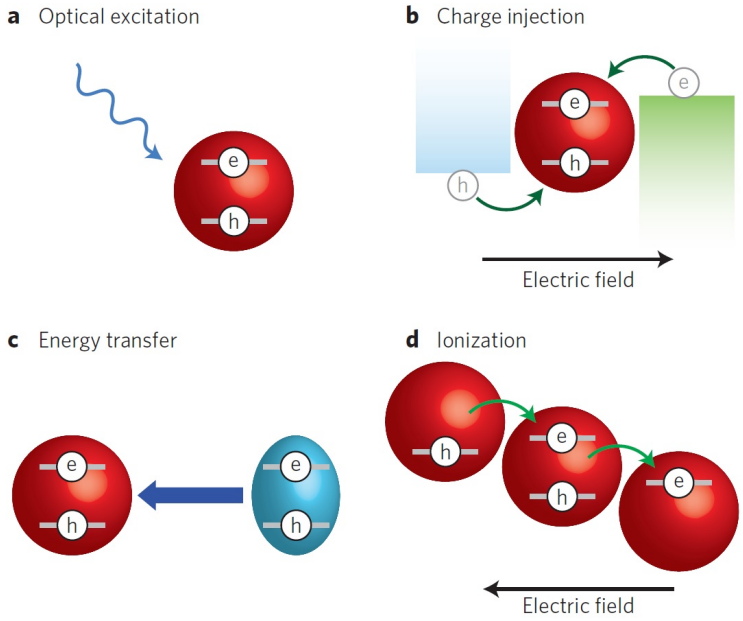

Figure 2.6: Various mechanisms of QD excitation: (a) optical excitation, (b) charge injection, (c) energy transfer, and (d) ionization [15].

The exciton can be generated in the four ways: optical excitation where an exciton is formed by absorption of a high-energy photon; charge injection where an exciton is formed by injection of electrons and holes from ETL and HTL respectively; energy transfer where an exciton is transferred to the active layer by Förster resonant energy transfer (FRET) and ionization where a large electric field ionizes an electron from one QD to another, thereby

generating a hole as shown in Figure 2.6 [28]. The two main mechanisms of excitation that govern the light emission from an electrically driven colloidal QD-LED are charge injection and FRET. In direct charge injection, electrons and holes are injected from the respective electrodes through the charge transport layers in the QD layer. The electron-hole pair recombines across the bandgap emitting light of characteristic wavelength. FRET is another dominant mechanism of QD excitation where the QD layer is in close proximity to organic polymers, small organic molecules or inorganic layers. In FRET, the electron-hole pairs formed in the charge transport layers transfer energy non-radiatively to the QD layer by dipole-dipole coupling [28]. The focus of this thesis is on direct charge injection as it is the most efficient method of injection carriers and moreover, if this QD-LED is to be integrated with a CMOS chip, they need to be electrically driven.

2.5 Device Design

In this thesis there were two devices designed for colloidal QD LEDs. As shown in Figure 2.7, the first QD LED structure consists of the following layers of inorganic materials: aluminum (Al) as the cathode, 40 nm of zinc oxide (ZnO) as the electron transport layer, CdSe/ZnS particles as the active layer, p-silicon as the hole transport layer and 200 nm of thick Al as an anode. The choice of silicon as a substrate should be quite obvious as we are trying to fabricate LEDs based on a silicon backplane. Apart from other motivations of using silicon as substrate, p-type silicon has been demonstrated to have enhanced hole injection compared to the indium–tin–oxide (ITO) anode [29]. The band diagram shown excludes the thin native oxide layer which acts as a buffer layer and enhances hole injection by dropping most of the electric field across the insulating oxide layer [30]. The presence of thin native oxide aligns the fermi level of the electrodes with the valence band of a semiconductor, thereby increasing the balance of carriers in the active layer increasing the probability of radiative recombination [30]. Aluminum has been used as contacts for the QD LED structure because

of its CMOS compatibility and also because its work function allows efficient injection of holes and electrons. It has also been demonstrated that device performance improved when using Al as contacts rather than Au/Ag (gold/silver) for a similar structures [31, 32]. A QD layer in contact with metal is easily quenched, hence a 40 nm ZnO layer is deposited which separates the two layers and further enhances the balance of holes and electrons in the active QD layer [31].

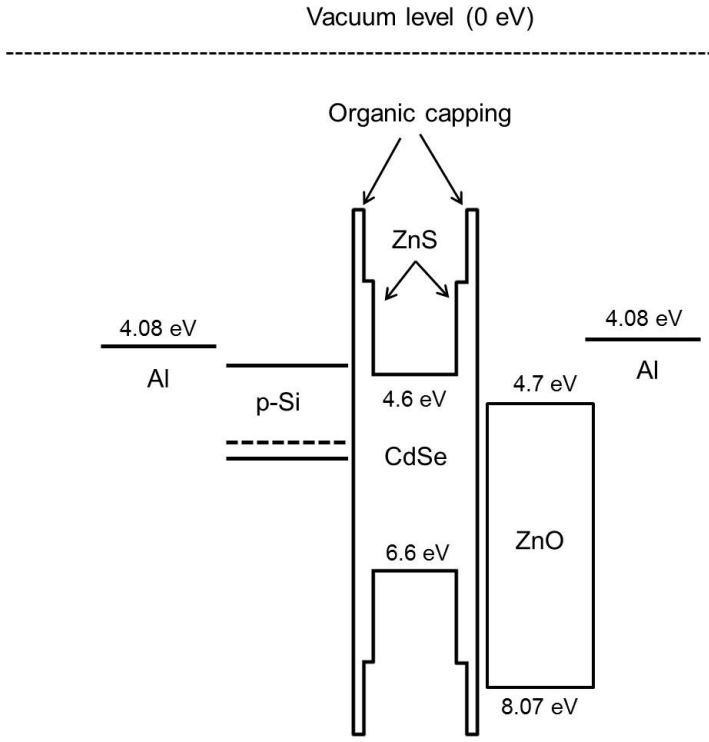

Figure 2.7: Schematic of the band diagram of the first QD-LED structure with no bias applied.

With the application of a forward bias voltage, the holes are injected from the Al anode through the p-type silicon and they tunnel through the oxide to the active QD layer. Likewise, electrons are injected from the Al layer and travel through the ZnO layer to the active QD layer. The small band offset in between the conduction band of the ZnO and the CdSe nanocrystals allows efficient electron injection and the large valence band offset blocks holes. The thin native oxide layer blocks the electrons from escaping the active layer. This structure allows the formation of electron-hole pairs in the active layer which recombine radiatively

emitting the wavelength of light corresponding to the nanocrystal size.

The band structure diagram of the second device structure with no bias is shown in Figure 2.8. It consists of layers of inorganic materials: Al as the cathode, 40 nm of zinc oxide (ZnO) as the electron transport layer, CdSe/ZnS particles as the active layer, 40 nm of nickel oxide (NiO) as the hole transport layer and p-type silicon with 200 nm of thick indium-tin oxide (ITO) as an anode. The materials are chosen so that the band offset allows the efficient injection of holes and electrons respectively while blocking them from escaping the active layer.

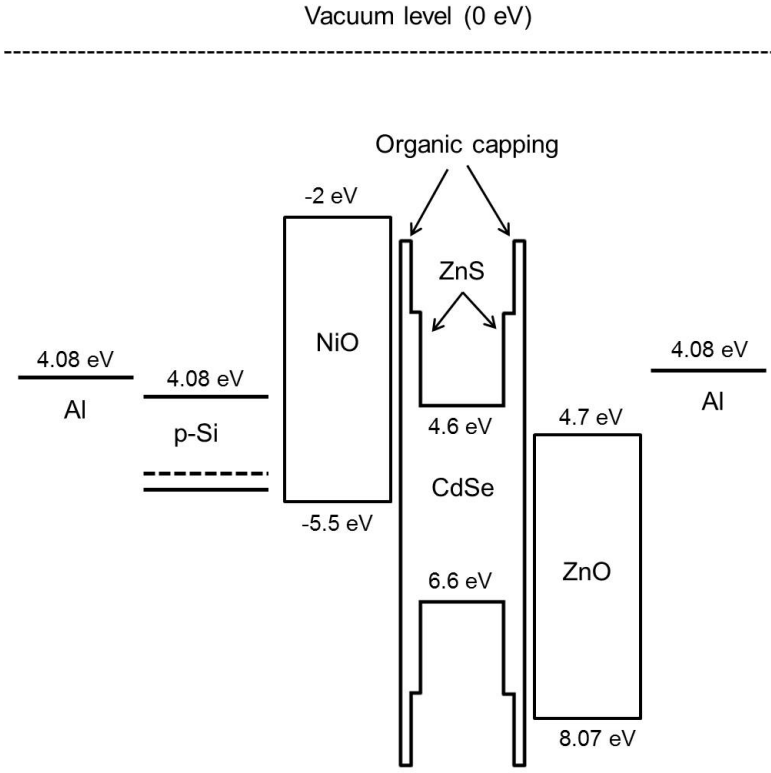

Figure 2.8: Schematic of the band diagram of the second QD-LED structure with no bias applied.

Similar to the first device structure, application of forward bias voltage to this inverted structure will induce an electric field across the device structure. The holes are injected from the Al anode through the p-type silicon and they travel through NiO to the active QD layer. Likewise, electrons are injected from the Al layer and travel through the ZnO

layer to the active QD layer. The NiO and ZnO have similar free carrier concentrations and energy-band offsets to the QDs which allow the electron and hole injection into the QD layer to be balanced and help prevent QD charging which results from excess of one type of carrier in the QD active layer [33]. This allows efficient radiative recombination of electron-hole and light emission.

Chapter 3

Fabrication and Results

3.1 Synthesis of Colloidal Quantum Dots

The most successful method of preparing nanocrystals of high quality and a high degree of monodispersity is by organo-metallic synthesis. This process involves combining an organo-metallic precursor with a corresponding chalcogen precursor in a boiling solvent at high temperatures as shown in Figure 3.1 [34].

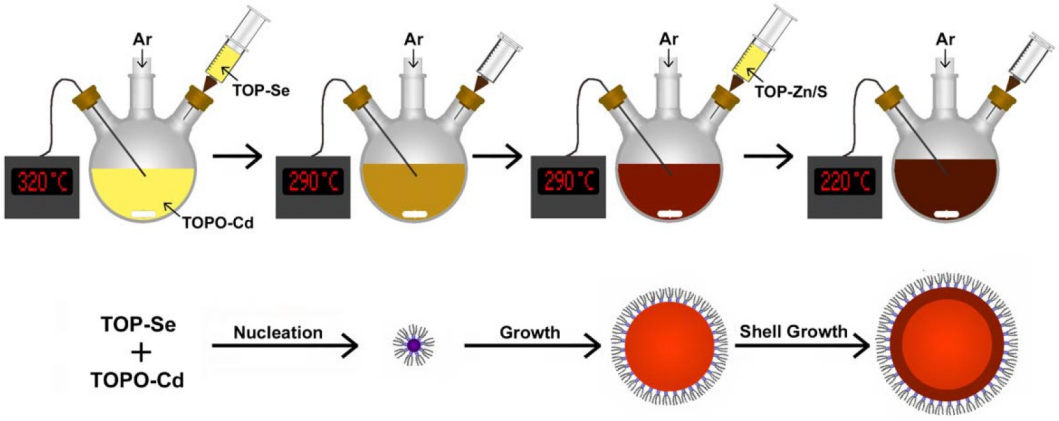

Figure 3.1: Synthesis of colloidal CdSe quantum dots [34].

A typical setup for preparation of nanocrystals includes a three-necked flask, a thermocouple with a controller to monitor and control the temperature, a heating mantle to heat the solvent and supply of argon gas to provide an inert atmosphere. The process of synthesis of dots begins by rapidly injecting precursor reagents such as zinc and cadmium into a hot

boiling solvent at high temperature (120 °C - 360 °C). The solvents that are commonly used are trioctylphosphine oxide (TOPO), trioctylphosphine (TOP), and octadecene which have high boiling points. The rapid injection of the precursor leads to nucleation and the temperature is decreased by injecting a room-temperature solution [13]. Then, the reaction enters the growth phase. Growth becomes faster with time, however Ostwald ripening [35] (the process of smaller particles being consumed by larger particles) and the long chain ligands tend to slow the aggregation process and eventually lead to the formation of monodisperse dots. The size of the QD can be monitored during the growth period using a spectroscopic probe within the reaction flask or by examining aliquots (a sample or a portion of the total amount of a solution) taken at various intervals [34]. The growth can be stopped once the desired size has been reached by simply taking out samples at certain times from the reaction flask. The growth rate and particle size values can be tuned by controlling the initial precursor concentration, the growth temperature and the length of the growth period or by introducing additional precursor material into the reaction vessel during the growth period [34]. After the desired size is obtained, the QDs are surface passivated to improve the fluorescence yield by the depositing an inorganic capping layer. The capping layer is obtained by injecting precursors such as zinc and sulphur dissolved in TOP. This capping layer forms the shell and is made of a semiconductor material of wider bandgap than the core material. These core-shell structures with efficient surface passivisation increase the probability of radiative recombination by providing better carrier confinement within the QD core. The QDs are stable in air although the reactions carried out to produce the QDs are performed under an inert atmosphere. This allows QD to be used relatively easily for various applications. Thus, using this process, the size and shape of the nanocrystals can be highly controlled by choosing the right precursor reagents, capping ligands and controlling the temperature and time.

3.2 Purification of Colloidal Quantum Dots

Nanocrystals are synthesized in hot organic solvents and have organic ligands attached to them. Therefore, they cannot be directly used to make electronic devices as these excess ligands and impurities impede carrier transport and reduce the efficiency of the device by forming a short-circuit between various nanocrystal films. They need to undergo a purification step before being used as a functional material for devices. Purification is carried out by precipitating the quantum dots using polar solvents like methanol/butanol or acetone [13]. The purification steps for CdSe/ZnS QDs coated with TOPO and TOP is outlined in the following:

1. The QDs are initially dissolved in a non-polar solvent such as hexane or toluene.
2. A fixed concentration of colloidal QD solution is taken in a glass tube and methanol is added until they precipitate. The colloidal QDs precipitate in polar solvents such as methanol, butanol etc. Methanol is added to the solution of colloidal QDs until they become cloudy.
3. The precipitate should then be centrifuged at 4000 rpm for approximately 3-4 minutes. As a result, QDs settle on the bottom of the tube and the supernatant (the liquid lying above a solid residue after precipitation and centrifugation) looks transparent.
4. The supernatant contains excess precursors and ligands and should be discarded. The QDs are dried by blowing air slowly using a nitrogen air gun.
5. The precipitants are then re-dispersed in a non-polar solvent such as toluene, chloroform, hexane etc. to obtain a clear solution of colloidal quantum dots. For use in electronic devices, the solution is purified multiple times following the steps mentioned above and the final solution is filtered using a polytetrafluoroethylene (PTFE) filter before use.

3.3 Deposition Techniques

Semiconductor nanocrystals need to be deposited or coated as a thin film to a surface so they can be used as a functional material to fabricate devices. Different methods of coating can be used depending on the necessary properties of the film desired such as thickness, uniformity, patterning and orientation of the nanocrystals. Some methods of depositing colloidal quantum dots are outlined in the following:

3.3.1 Spin Casting

This is a simple method of depositing a thin layer of colloidal quantum dots. Even a monolayer of quantum dots can be achieved by spin casting a solution of QDs in a low boiling point solvent onto the substrate [13]. In spin casting, the solution is placed on the substrate for 2 minutes to wet the entire surface and is spun at a speed greater than 1000 rpm. The drawback of this method is that the majority of solution is lost due to the centrifugal force while spinning.

3.3.2 Drop Casting

Drop casting is the simplest method for coating colloidal quantum dots. In drop casting, a drop of colloidal solution is poured on the substrate and is allowed to dry. This method leads to the formation of a multilayer of close-packed quantum dots. The surface resulting from drop casting is very rough and is generally not applicable for fabricating stacked structures for devices.

3.3.3 Microcontact Printing

Microcontact printing is another method for depositing colloidal quantum dots which yields uniform surface coating. It involves spin coating the colloidal solution suspended

in organic solvent onto a polydimethylsiloxane (PDMS) stamp coated with a thin film of paralene-C and stamping the result onto the substrate. This process is illustrated in the Figure 3.2.

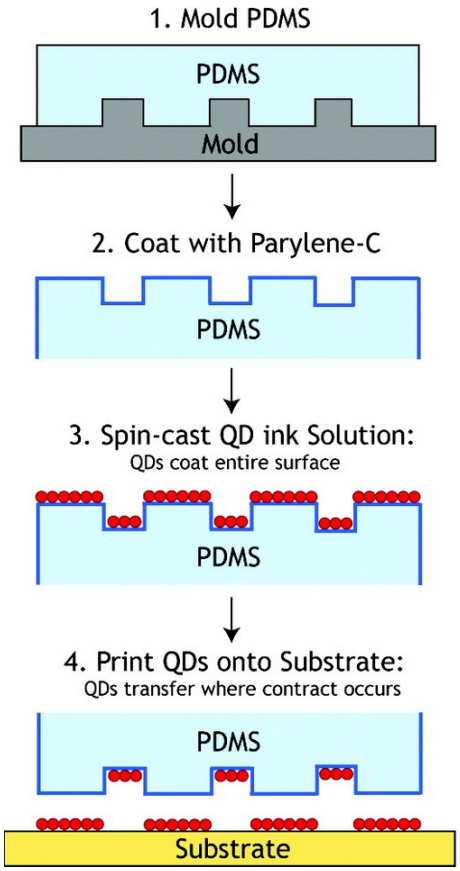

Figure 3.2: Schematic showing the process of microcontact printing [36].

3.3.4 Inkjet Printing

Inkjet printing is a form of drop cast printing which is used for depositing colloidal solutions for large area electronic applications as it reduces the use of material and allows multiple deposition of high-resolution patterned layers. Since this method uses a drop cast mechanism for deposition, it results in non-uniformity of film due to the "coffee-ring" phenomenon. A two-solvent technique has been used to improve uniformity in film and facilitate deposition.

3.3.5 Langmuir-Blodgett Technique

In this method, a Langmuir trough with water is covered by a solution of QDs. The colloidal QDs are not soluble in water so they float on the surface and these QDs are squeezed into the center by moving the trough walls closer together. The quantum dots are then picked up using a PDMS stamp and printed on substrates through contact.

3.4 Lithographic Patterning Colloidal Quantum Dots

The patterning of colloidal QDs at sub-micron and nanometer resolution is essential for various applications in photonics and plasmonics. Many applications of colloidal QDs are still based on spinning dilute solutions of quantum dots on a desired substrate. This method results in random distribution of dots which leads to poor device performance. More recently, various methods of patterning the colloidal QDs have been reported. A few popular methods include microcontact printing, self-assembly and ebeam lithography. Microcontact printing involves spin casting colloidal QDs on a paralyene coated PDMS (Polydimethylsiloxane) stamp which allows deposition of multiple monolayers of QDs on various substrates [36]. However, microcontact printing is limited by the resolution of the PDMS stamp and it is extremely difficult to pattern QD clusters on a pre-defined structure without alignment mismatch [37]. Sub-nanometer resolution patterning has been demonstrated using electrostatic force mediated self-assembly [38], however, this approach becomes difficult for patterning thicker QD clusters or multiple QD layers [37]. This section of the thesis explains patterning of colloidal quantum dots using ebeam lithography and the conventional liftoff process. Ebeam patterning can be ultimately used for patterning single QDs which would help study single-dot properties of colloidal QDs [39].

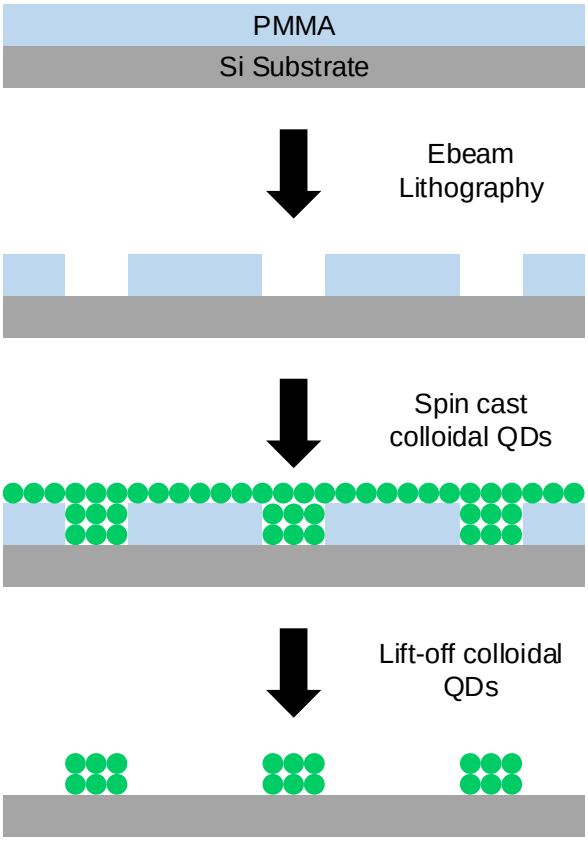

Figure 3.3: Fabrication process of ebeam patterning of colloidal QDs.

The major steps involved in the fabrication and liftoff of colloidal QDs is demonstrated in Figure 3.3. The ebeam lithography was carried out by spin coating a 40 nm thick polymethylmethacrylate (PMMA) resist on a silicon substrate. The resist was then baked at 200 °C for 2 minutes on a hotplate. Then, patterns with straight lines of 200 nm width with various pitch-widths of 10 μm and 300 μm were exposed on PMMA by ebeam lihtography. After exposure the PMMA was developed to obtain the patterns as desired. Then, CdSe/ZnS QDs dissolved in toluene were purified about 3 times following the procedure described in section 3.2. The purified QD solution was then spin casted on the patterned substrate at 800 rpm for 40 seconds. The sample was then heated at 90 °C for 5 minutes. Then, the liftoff was carried out by dipping the sample in acetone for 3-4 minutes. SEM images were taken to verify the success of the liftoff process. The SEM images are shown in Figure 3.4 and Figure 3.5.

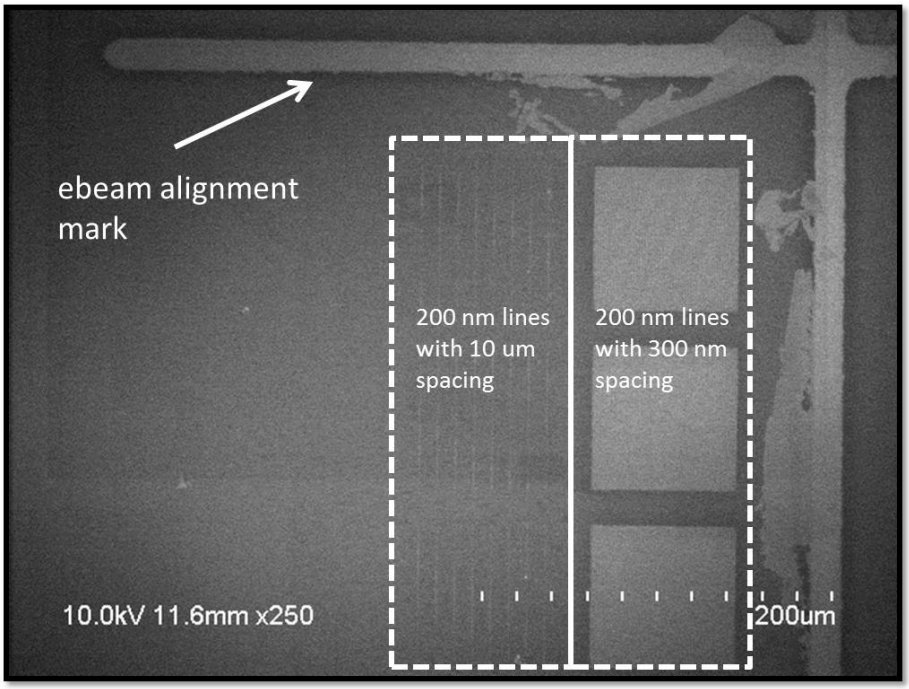

Figure 3.4: SEM image of ebeam patterned colloidal QD after liftoff.

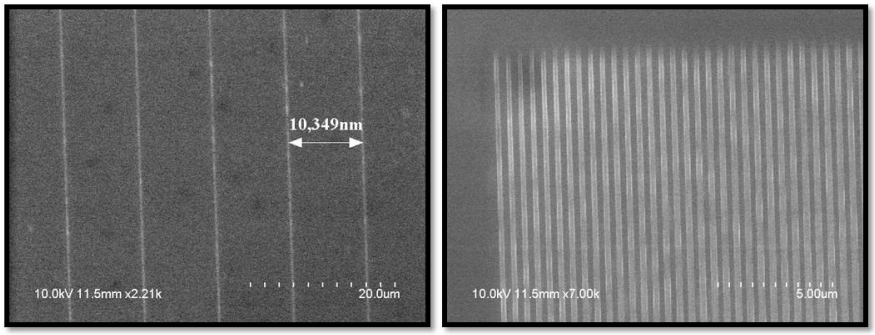

Figure 3.5: Higher magnification SEM image of ebeam patterned colloidal QDs.

The technique described above demonstrates the ability to control the placement of QD clusters using ebeam lithography. Further PL tests were conducted to verify that colloidal QDs were still optically active after liftoff. This nanoscale patterning process would ultimately allow integration of individual QDs in optoelectronic systems.

3.5 Overall Device Fabrication

This section describes the fabrication of various colloidal QD-based LEDs in detail. The fabrication of a typical colloidal QD LED involves patterning and depositing a colloidal QD layer, depositing charge transport layers and contacts to inject charges efficiently. This section describes the recipe and fabrication tools used for fabricating colloidal QD LEDs.

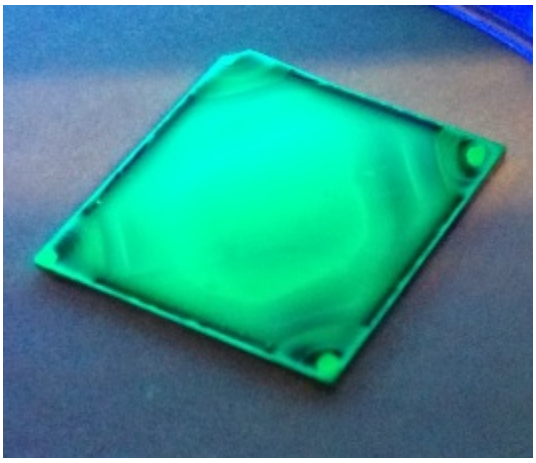

Figure 3.6: Sample under UV excitation after spin-coating the colloidal QDs.

The colloidal QD-LEDs are based on silicon backplane and the silicon used in this thesis was a <100> p-type with a resistivity of 1-10 Ohm-cm. The fabrication process started with solvent cleaning the silicon wafer with acetone at 55 °C for 10 minutes, methanol for 5 minutes and rinsing with DI water. The silicon wafer after cleaning was baked for 1 minute at 125 °C for dehydration and then cleaved into 12 mm x 12 mm pieces. The samples were then put into a radio frequency (RF) sputterer and the back side of the samples were sputtered with Al at a power of 200 W for 20 minutes under argon (Ar) atmosphere. This process yielded 225 nm of thick Al coating on the back used for back contact. The back contact was then annealed at 400 °C for 60 seconds using a Jipelec RTP (rapid thermal processor) under N_2 atmosphere which helps avoid further oxidation of metal during annealing and can also reduce any interfacial oxide between the metal and semiconductor. High-temperature annealing reduces the barrier at the metal-semiconductor interface and thereby reducing the

contact resistivity. To ensure a Ohmic contact one sample was prepared with 10 nm of Al for front contact and the J-V curve was plotted using a semiconductor parametric analyzer.

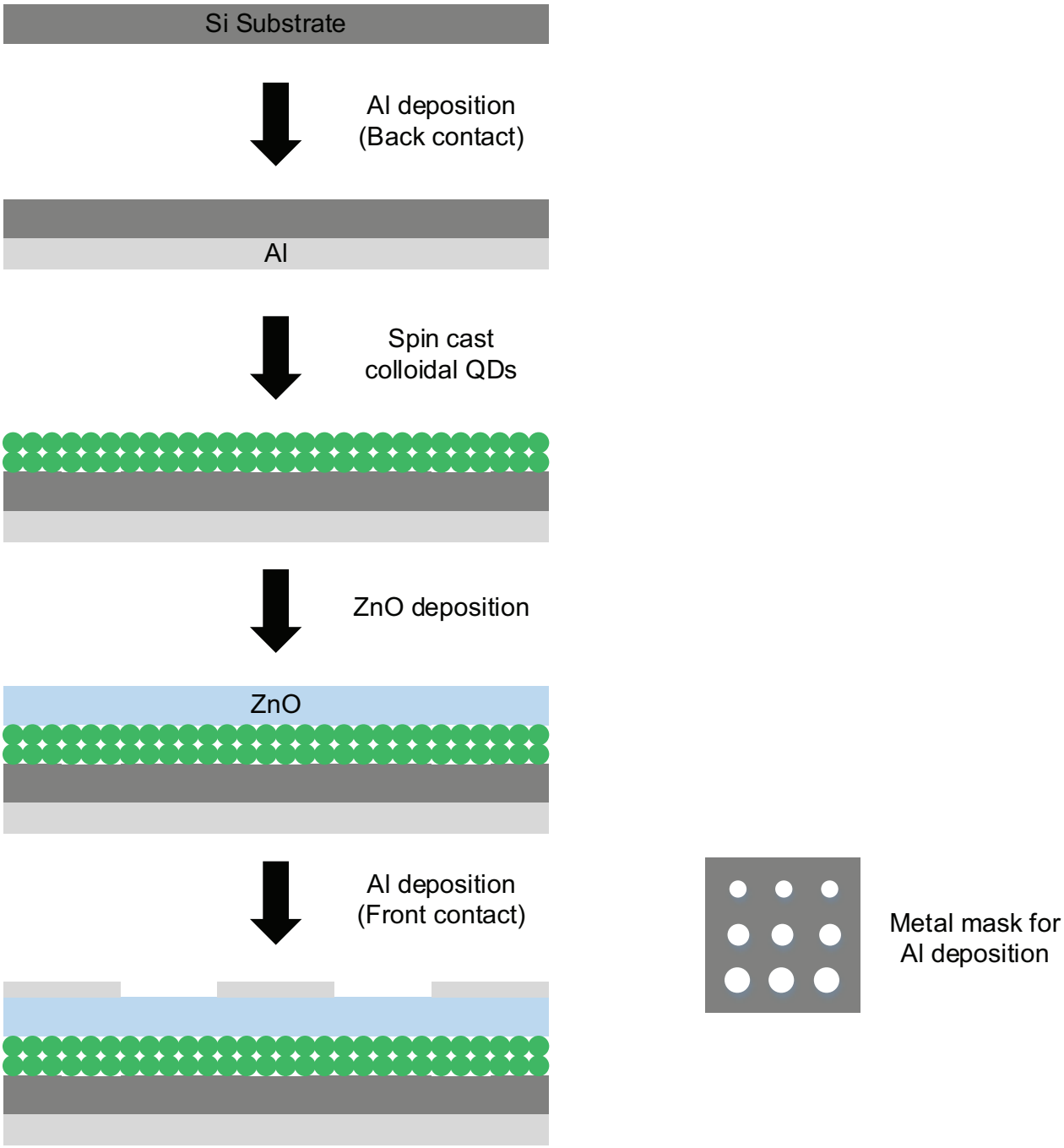

Figure 3.7: Fabrication steps for colloidal QD LEDs.

The samples with backside Al contact are then spin coated with CdSe/ ZnS colloidal QDs

at 800 rpm for 40 seconds. The colloidal QDs used were bought from Sigma Aldrich and had a concentration of 5 mg/ml in toluene. For fabrication, 1 ml of this original solution was purified as above and the precipitate was dissolved in 0.5 ml of toluene. The QD solution was then filtered using a PTFE filter. The sample was then baked at 110 °C for 10 minutes. Figure 3.6 shows an image of a sample under ultravoilet (UV) excitation which was prepared by spin coating CdSe/ZnS (465 nm) colloidal QD solution and annealed at 110 °C for 10 minutes.

ZnO was sputtered using a Cooke dual-gun sputter system. The samples are loaded and the chamber is pumped down to a pressure of 2000 millitorr. Since the ZnO layer is deposited on top of colloidal QD, low power of 50 W was used for sputtering in order to avoid damage to the colloidal QD layer. The sputtering was carried out for 20 minutes depositing 40 nm of ZnO.

Finally a thin layer of Al for the front contact was deposited using the sputter. The chamber pressure was around 2000 millitorr and the power was raised to 200 W. The deposition was carried out for 2 minutes. The devices were then forward biased using a probe station connected to a power supply and testing for operation was carried out. The schematic of the entire fabrication is shown in Figure 3.7.

3.6 Results

In this thesis, LEDs were fabricated using CdSe/ZnS core/shell colloidal QDs of two different emission wavelengths. The colloidal QD with an emission wavelength of 485 nm (blue) was obtained from Sigma Aldrich whereas the colloidal QD with an emission wavelength of 630 nm (red) was obtained from Ocean Nanotech. These colloidal QDs were purified and dissolved in toluene before measuring the emission and absorption spectra. The emission and absorption spectra of the two colloidal QDs were measured using fluorescence spectrophotometer and UV-Vis-NIR spectrophotometer respectively.

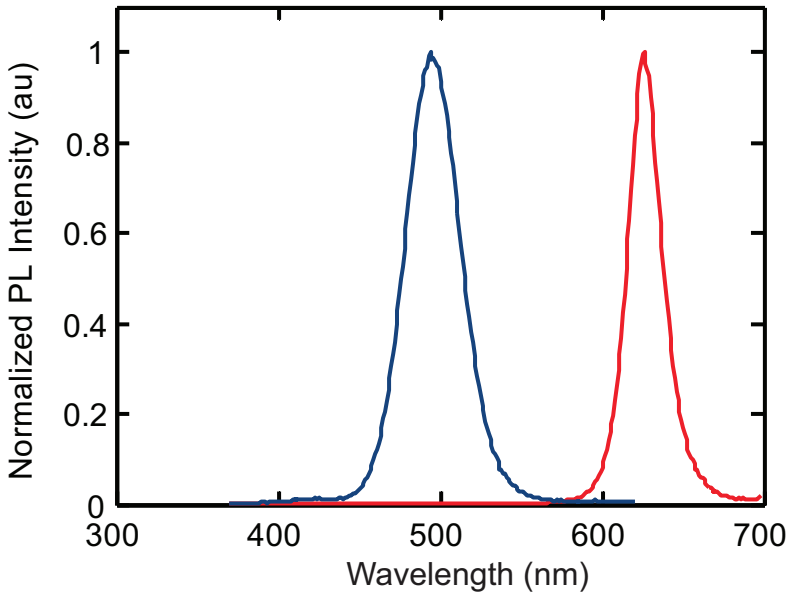

Figure 3.8: Photo-luminescence spectrum of CdSe/ZnS colloidal QDs dissolved in toluene with emission wavelength of 485 nm (blue) and 630 nm (red).

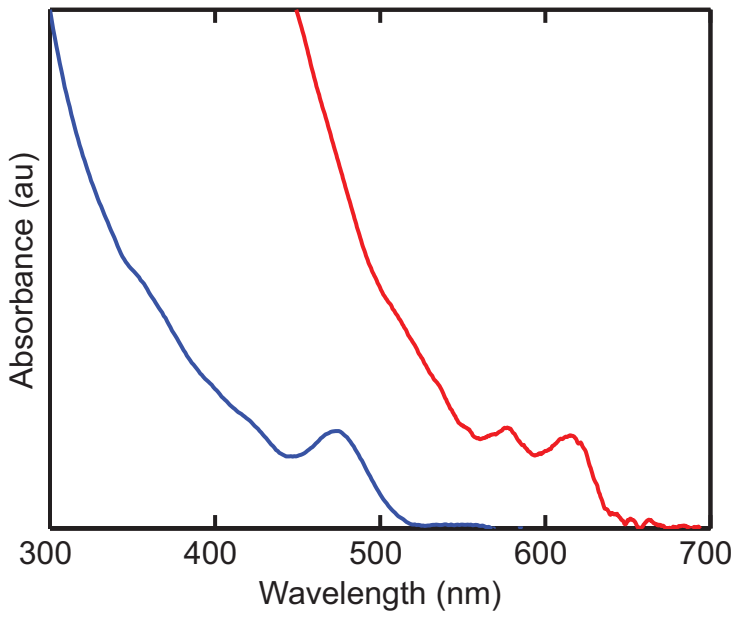

Figure 3.9: Absorption spectrum of CdSe/ZnS colloidal QDs dissolved in toluene with emission wavelengths of 485 nm (blue) and 630 nm (red).

From the emission spectra of the colloidal QDs as shown in Figure 3.8, the emission peak of the blue and red colloidal QDs and the FWHM (full width at half maximum) of around

40 nm and 25 nm can be noted respectively. The absorption spectra as shown in Figure 3.9 shows sharp transitions representing the discrete quantized energy states along with the blue shift in wavelength with the decrease in diameter of the quatum dots (diameter of blue QD is less than red QD).

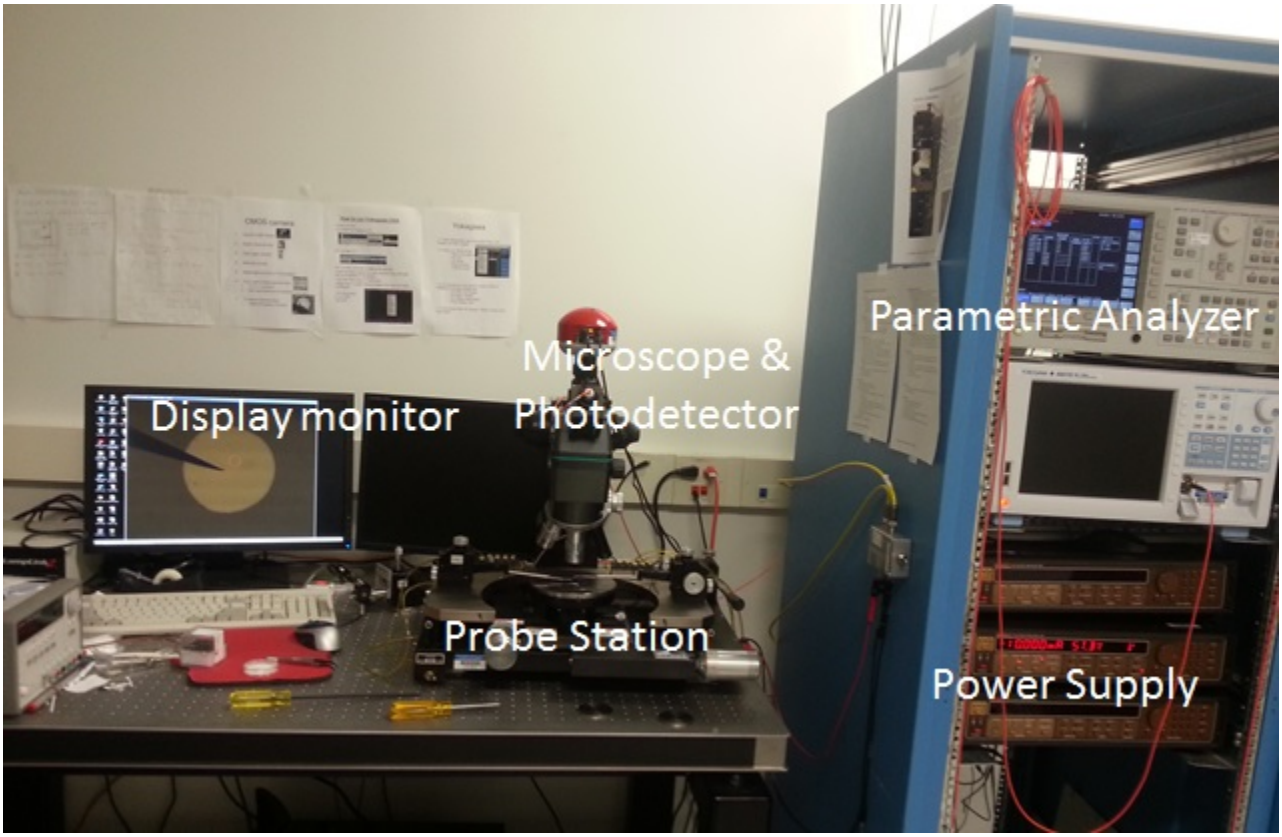

Figure 3.10: Photograph of the experimental setup used for testing colloidal QD LEDs.

After the LEDs were fabricated, they were tested for emission using the setup shown in Figure 3.10. The setup consisted of a probe station with a display monitor where the sample was placed for probing. The sample was probed applying a negative bias on the top contact using a power supply and a bottom contact was grounded by grounding the plate of the probe station. The semiconductor analyzer was used for recording the IV characteristics of the various samples. The IV curve of a colloidal QD LED with an emission wavelength of 485 nm, fabricated by the above mentioned process except for the patterning is shown in Figure 3.11.

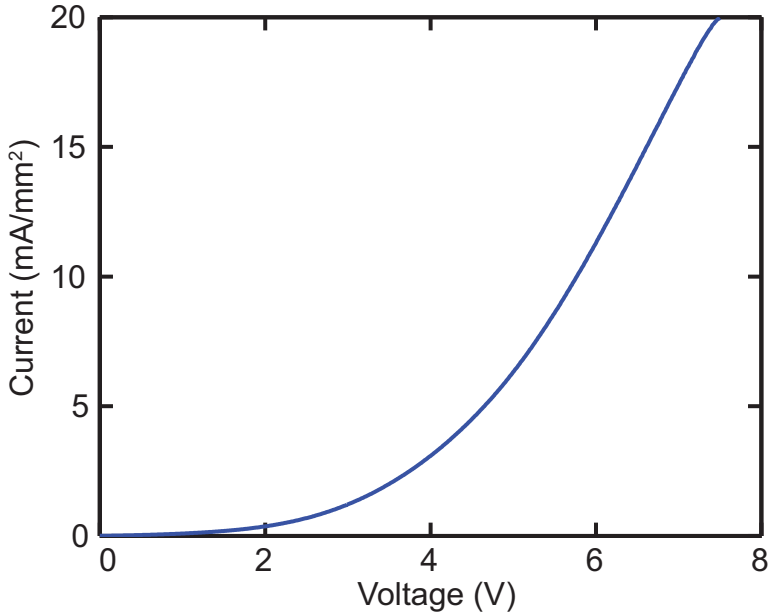

Figure 3.11: J-V curve of colloidal QD-LED withemission wavelength of 485 nm (blue).

The figure shows that the device has a modest turn on voltage of around 2 V. Since an LED is a current-dependent device with light output intensity being directly proportional to the current flowing through it, it requires a current to flow through it before it can emit any light. In this investigation, only the samples which were not patterned emitted light. These samples had a 50 nm thick top metal contact and light emission could only be observed at the edges of the sample. On the other hand, samples that were patterned as described in section 3.5 did not emit light. These samples had very thin top metal contact (10 nm) and the metal was deposited establishing hard contact between the sample and the metal mask. The failure of light emission from these samples with metal patterns on top can be attributed to electric-field induced QD luminescence quenching and QD charging. The thin metal layer on top of the patterned samples brings the QD layer close to the material interfaces, where electric fields are typically very high [28]. This increases the exposure of high electric fields to the QD layer and causes QD luminescence quenching. Another reason for failure of light emission is QD charging which occurs whenever DC current is passed through the QD layer. The charged QD layer makes passing the current through the device extremely difficult which

makes maintaining electro-luminescence harder. From these results, the recommendation is that QD-LEDs should be designed in such a way that the QD layer is placed away from material interfaces and high electric field regions [28].

Among other parameters the performance of an LED can be further characterised by calculating efficiency, responsivity, and brightness. Here, a few important LED performance parameters are discussed.

Internal quantum efficiency (η_i): All the carriers injected into the active layer of an LED do not recombine radiatively. The carriers in the active region can recombine nonradiatively thus reducing the efficiency. The internal quantum efficiency is defined as the ratio of generated photon flux to the injected electron flux and is expressed as [40]:

$$\eta_i = \frac{number\,of\,photons\,generated\,per\,sec}{number\,of\,electrons\,injected\,into\,LED\,per\,sec} = \frac{\left(\frac{P_{int}}{hv}\right)}{\left(\frac{I}{e}\right)} \tag{3.1}$$

where P_{int} is the optical power injected into the active layer of the LED, e is the magnitude of electronic charge, and I is the current injected into the device. In order to increase the internal quantum efficiency, the active layer in our case collodial QD of high crytalline purity with minimum defect and trap states along with high quantum yield should be used.

Extraction efficiency (η_e): The photons generated in the active region of an LED is radiated in all directions uniformly in free space. However, the photon flux from the device depends on the direction of emission which for a real device is effected by reabsorption and total internal reflections. Therefore, the extraction efficiency of an LED is defined as the efficiency with which the photons generated in the active region can be extracted from the device and is expresssed as [40]:

$$\eta_e = \frac{number\,of\,photons\,emitted\,in\,free\,space\,per\,sec}{number\,of\,photons\,generated\,per\,sec} = \frac{\left(\frac{P}{hv}\right)}{\left(\frac{P_{int}}{hv}\right)} \tag{3.2}$$

where P is the optical power emitted free space. In order to increase the extraction efficiency, antireflection coatings are used to reduce Fresnel reflection.

External quantum efficiency (η_{ex}): The external quantum efficiency of an LED is defined as the ratio of the number of photons emitted into free space to the number of injected carriers. It is a very important LED performance parameter and is expresssed as [40]:

$$\eta_{ex} = \frac{number\,of\,photons\,emitted\,per\,sec}{number\,of\,electrons\,injected\,into\,LED\,per\,sec} = \frac{\left(\frac{P}{hv}\right)}{\left(\frac{I}{e}\right)} = \eta_i \times \eta_e \tag{3.3}$$

Power conversion efficiency (η_p): The power efficiency or the wall plug efficiency is the ratio of emitted optical power to the applied electrical power and is expressed as [40]:

$$\eta_p = \frac{(P)}{(IV)} = \frac{number\,of\,photons\,emitted\,externally}{IV} \times hv \tag{3.4}$$

where I is the current flowing through the LED and V is the voltage drop across the device. The power efficiency becomes equal to the external efficiency if the operational voltage of the device is approximately equal to the energy gap of the semiconductor, i.e. if $hv \sim eV$ then $\eta_p \sim \eta_{ex}$.

Responsivity (R): The responsivity of an LED is defined as the ratio of the optical power emitted to the injected current and is expressed as:

$$R = \frac{P}{I} = \frac{hv}{e} \times \eta_e \tag{3.5}$$

There is a linear dependence of the LED output power on the injected current but it is valid only when the current is less than a certain value (few mA for typical LEDs). When the current increases, the device reaches the saturation and causes the linear proportionality to fail. This phenomenon is called "efficiency droop" which is caused due to electron leakage. With the increase in current an electric field develops within the p-type region of the diode,

allowing electrons to escape the active region despite high barriers that confine the carriers in the active region [41].

Chapter 4

Conclusions and Future Direction

4.1 Thesis Summary

In this thesis, design and fabrication of colloidal QD-based light-emitting devices on silicon substrate have been described. This thesis demonstrated the ability to integrate colloidal QDs with silicon which would allow the use of established advance CMOS technology. The use of CMOS technology would in turn allow high volume manufacturing of compact light sources used in optical communication. The unique properties of colloidal QDs such as wide tunability, high photoluminescence (PL) efficiency make the QDs a great candidate for using as an active material in the light-emitting devices. Colloidal QDs also allowed solution processability which makes integration with a silicon platform very effective.

The materials for the device structure were chosen to ensure the efficient injection of charges. The device structure consisted of p-type silicon, CdSe/Zns as the active material, SiO_2 as the hole transport layer and ZnO as the electron transport layer, respectively, and finally Al as contacts. The colloidal QD used forms a type I heterojunction which allows confinement of charge carriers and increases the probability of radiative recombination. The hole and electron transport have higher bandgaps than the active material, thus allowing efficient injection of charges into the active region. The device fabrication involved deposition of colloidal QDs using spin coating and further sputtering of ZnO and Al layers for charge transport and contact respectively. The devices that were not patterned showed steady emission of light when forward biased with a turn on voltage of 2 V whereas patterned

devices with a thin top electrode failed to emit light due to QD charging and QD luminescence quenching.

Along with design and fabrication, patterning of colloidal QDs is extremely important for creating efficient LEDs. This thesis presented various methods which could be used for effectively patterning quantum dots. The most effective way of patterning these dots for micron resolution has been through micro-contact printing. This thesis also demonstrated the failure of colloidal QDs liftoff after photolithography, but on the other hand, successfully demonstrated nanoscale patterning of colloidal QDs using ebeam lithography. The nanoscale patterning allows controlled placement of these colloidal QDs used for various single photonic and plasmonic applications.

4.2 Future Direction

In this thesis, we demostrated the ability to integrate colloidal QDs with silicon substrate to create patterned LEDs for visible wavelengths of 435 nm and 630 nm. This section will outline some future direction and challenges to overcome in order to develop colloidal QD-based LEDs on silicon for an optical communication wavelength (1330 nm and 1550 nm). The first logical step would be to use infrared colloidal QDs with high quantum photoluminescence efficiency such as PbSe or PbS emitting light in the optical communication window. The next big challenege would be to improve the efficiency of these devices to the level of commercially available LEDs. The key to developing an efficient infrared colloidal QD LED would be through intelligent device design, improving the photon output coupling and understanding the fundamental operating mechanisms. The design could be further improved by using colloidal QDs or even colloidal nanorods with higher quantum yield, using QD with high-dielectric encapsulation which reduces QD luminescence quenching, using contacts that allow efficient current injection, and also using transparent contacts such as ITO, graphene could increase the overall efficiency.

Bibliography

[1] B. Jalali and S. Fathpour, "Silicon photonics," *Journal of Lightwave Technology*, vol. 24, no. 12, pp. 4600–4615, 2006.

[2] Y. A. Vlasov, "Silicon CMOS-integrated nano-photonics for computer and data communications beyond 100G," *Communications Magazine, IEEE*, vol. 50, no. 2, pp. 67–72, 2012.

[3] D. Liang and J. E. Bowers, "Recent progress in lasers on silicon," *Nature Photonics*, vol. 4, no. 8, pp. 511–517, 2010.

[4] M. A. Green, J. Zhao, A. Wang, P. J. Reece, and M. Gal, "Effcient silicon light-emitting diodes," *Nature*, vol. 412, pp. 805–808, 2001.

[5] H. Rong, R. Jones, A. Liu, O. Cohen, D. Hak, A. Fang, and M. Paniccia, "A continuous-wave Raman silicon laser," *Nature*, vol. 433, pp. 725–728, 2005.

[6] W. L. Ng, M. A. Lourenc, R. M. Gwilliam, S. Ledain, S. G., and K. P. Homewood, "An efficient room-temperature silicon-based light-emitting diode," *Nature*, vol. 410, pp. 192–194, 2001.

[7] R. J. Walters, G. I. Bourianoff, and H. A. Atwater, "Field-effect electroluminescence in silicon nanocrystals," *Nature Materials*, vol. 4, no. 2, pp. 143–146, 2005.

[8] N. Daldosso, D. Navarro-Urrios, M. Melchiorri, C. Garcia, P. Pellegrino, B. Garrido, C. Sada, G. Battaglin, F. Gourbilleau, and R. Rizk, "Er-coupled Si nanocluster wave-guide," *IEEE Journal of Selected Topics in Quantum Electronics*, vol. 12, no. 6, pp. 1607–1617, 2006.

[9] H. Park, A. W. Fang, S. Kodamaa, and J. E. Bowers, "Hybrid silicon evanescent laser fabricated with a silicon waveguide and III-V offset quantum wells," *Optics Express*, vol. 13, pp. 9460–9464, 2005.

[10] M. Hochberg, N. C. Harris, R. Ding, Y. Zhang, A. Novack, Z. Xuan, and T. Baehr-Jones, "Silicon photonics: The next fabless semiconductor industry," *Solid-State Circuits Magazine, IEEE*, vol. 5, no. 1, pp. 48–58, 2013.

[11] P. Guyot-Sionnest, "Electrical transport in colloidal quantum dot films," *The Journal of American Physical Chemistry*, vol. 3, pp. 1169–1175, 2012.

[12] S. Ke, M. Vasudev, H.-S. Jung, J. Yang, A. Kar, Y. Li, P. Reinhardt, Kitt Snee, M. A. Stroscio, and M. Dutta, "Applications of colloidal quantum dots," *Microelectronics Journal*, vol. 40, pp. 644–649, 2009.

[13] J. E. Halpert, Design and synthesis of nanocrystal heterostructures for optoelectronic applications. Ph.D. dissertation, Massachusetts Institute of Technology, 2008.

[14] C. Murray, S. Sun, W. Gaschler, H. Doyle, T. Betley, and K. C.R., "Colloidal synthesis of nanocrystals and nanocrystal superlattices," *IBM Journal of Research and Development*, vol. 45, pp. 47–56, 2001.

[15] Y. Shirasaki, G. J. Supran, M. G. Bawendi, and V. V. Bulovic, "Emergence of colloidal quantum-dot light-emitting technologies," *Nature Photonics*, vol. 7, pp. 13–23, 2012.

[16] S. Coe-Sullivan, "Quantum dot development," *Nature Photonics*, vol. 3, pp. 315–316, 2009.

[17] C. Dang, J. Lee, C. Breen, J. S. Steckel, S. Coe-Sullivan, and A. Nurmikko, "Red, green and blue lasing enabled by single-exciton gain in colloidal quantum dot films," *Nature Nanotechnology*, vol. 7, pp. 335–339, 2012.

[18] T. Rauch, M. Böberl, S. F. Tedde, J. Fürst, M. V. Kovalenko, G. Hesser, U. Lemmer, W. Heiss, and O. Hayden, "Near-infrared imaging with quantum-dot-sensitized organic photodiodes," *Nature Photonics*, vol. 3, pp. 332–336, 2009.

[19] S. Keuleyan, E. Lhuillier, V. Brajuskovic, and P. Guyot-Sionnest, "Mid-infrared HgTe colloidal quantum dot photodetectors," *Nature Photonics*, vol. 5, pp. 489–493, 2011.

[20] V. Sukhovatkin, S. Hinds, L. Brzozowski, and E. H. Sargent, "Colloidal quantum-dot photodetectors exploiting multiexciton generation," *Science*, vol. 324, pp. 1542–1544, 2009.

[21] J. J. Coleman, J. D. Young, and A. Garg, "Semiconductor quantum dot lasers: A tutorial," *Journal of Lightwave Technology*, vol. 29, pp. 499–510, 2011.

[22] A. P. Alivisatos, "Semiconductor clusters, nanocrystals, and quantum dots," *Science*, vol. 271, p. 933, 1996.

[23] L. E. Brus, "Electron–electron and electron-hole interactions in small semiconductor crystallites: The size dependence of the lowest excited electronic state," *The Journal of Chemical Physics*, vol. 80, p. 4403, 1984.

[24] C. Murray, C. Kagan, and M. Bawendi, "Synthesis and characterization of monodisperse nanocrystals and close-packed nanocrystal assemblies," *Annual Review of Materials Science*, vol. 30, no. 1, pp. 545–610, 2000.

[25] V. I. Klimov, *Semiconductor and Metal Nanocrystals: Synthesis and Electronic and Optical Properties*, vol. 87. New York, NY: CRC Press, 2003.

[26] R. Marcus, "Chemical and electrochemical electron-transfer theory," *Annual Review of Physical Chemistry*, vol. 15, no. 1, pp. 155–196, 1964.

[27] A. M. Kuznetsov and J. Ulstrup, *Electron Transfer in Chemistry and Biology: An Introduction to the Theory*. Chichester: Wiley, 1999.

[28] Y. Shirasaki, G. J. Supran, M. G. Bawendi, and V. Bulović, "Emergence of colloidal quantum-dot light-emitting technologies," *Nature Photonics*, vol. 7, no. 1, pp. 13–23, 2012.

[29] X. Zhou, J. He, L. Liao, M. Lu, Z. Xiong, X. Ding, X. Hou, F. Tao, C. Zhou, and S. Lee, "Enhanced hole injection in a bilayer vacuum-deposited organic light-emitting device using a p-type doped silicon anode," *Applied Physics Letters*, vol. 74, no. 4, pp. 609–611, 1999.

[30] I. Parker and H. H. Kim, "Fabrication of polymer light-emitting diodes using doped silicon electrodes," *Applied Physics Letters*, vol. 64, no. 14, pp. 1774–1776, 1994.

[31] A. Gopal, K. Hoshino, S. Kim, and X. Zhang, "Multi-color colloidal quantum dot based light emitting diodes micropatterned on silicon hole transporting layers," *Nanotechnology*, vol. 20, no. 23, p. 235201, 2009.

[32] A. Gopal, K. Hoshino, and X. Zhang, "Photolithographic patterning of subwavelength top emitting colloidal quantum dot based inorganic light emitting diodes on silicon," *Applied Physics Letters*, vol. 96, no. 13, p. 131109, 2010.

[33] J. Caruge, J. Halpert, V. B. V Wood, and M. Bawendi, "Colloidal quantum-dot light-emitting diodes with metal-oxide charge transport layers," *Nature Photonics*, vol. 2, no. 4, pp. 247–250, 2008.

[34] R. E. Bailey, A. M. Smith, and S. Nie, "Quantum dots in biology and medicine," *Physics E*, vol. 25, pp. 1–12, 2004.

[35] B. Dickerson, D. Irving, E. Herz, R. Claus, W. Spillman, and K. Meissner, "Synthesis kinetics of CdSe quantum dots in trioctylphosphine oxide and in stearic acid," *Applied Physics Letters*, vol. 86, p. 171915, 2005.

[36] L. Kim, P. O. Anikeeva, S. A. Coe-Sullivan, J. S. Steckel, M. G. Bawendi, and V. Bulovic, "Contact printing of quantum dot light-emitting devices," *Nano Letters*, vol. 8, no. 12, pp. 4513–4517, 2008.

[37] Y. Park, Y.-G. Roh, U. J. Kim, D.-Y. Chung, H. Suh, J. Kim, S. Cheon, J. Lee, T.-H. Kim, and K.-S. Cho, "Nanoscale patterning of colloidal quantum dots on transparent and metallic planar surfaces," *Nanotechnology*, vol. 23, no. 35, p. 355302, 2012.

[38] Q. Zhang, C. Dang, H. Urabe, J. Wang, S. Sun, and A. Nurmikko, "Large ordered arrays of single photon sources based on II-VI semiconductor colloidal quantum dot," *Optics Express*, vol. 16, no. 24, pp. 19592–19599, 2008.

[39] V. R. Manfrinato, D. D. Wanger, D. B. Strasfeld, H.-S. Han, F. Marsili, J. P. Arrieta, T. S. Mentzel, M. G. Bawendi, and K. K. Berggren, "Controlled placement of colloidal quantum dots in sub-15 nm clusters," *Nanotechnology*, vol. 24, no. 12, p. 125302, 2013.

[40] D. V. Talapin, J.-S. Lee, M. V. Kovalenko, and E. V. Shevchenko, "Prospects of colloidal nanocrystals for electronic and optoelectronic applications," *Chemical Reviews*, vol. 110, no. 1, p. 389, 2010.

[41] D. S. Meyaard, G. Lin, J. Cho, E. Fred Schubert, H. Shim, S. Han, M. Kim, C. Sone, and Y. Sun Kim, "Identifying the cause of the efficiency droop in GaInN light-emitting diodes by correlating the onset of high injection with the onset of the efficiency droop," *Applied Physics Letters*, vol. 102, no. 25, p. 251114, 2013.